International Journal of Solids and Structures 46 (2009) 1491–1498

Contents lists available at ScienceDirect

International Journal of Solids and Structures

journal homepage: www.elsevier.com/locate/ijsolstr

Computational modeling of domain wall interactions with dislocations in ferroelectric crystals

Antonios Kontsos, Chad M. Landis *

Department of Aerospace Engineering and Engineering Mechanics, University of Texas at Austin, 210 East 24th Street, 1 University Station, C0600, Austin, TX 78712-0235, USA

ARTICLE INFO

Article history:
Received 16 September 2008
Received in revised form 19 November 2008
Available online 9 December 2008

Keywords:
Ferroelectrics
Phase-field modeling
Finite element methods
Domain walls
Dislocations

ABSTRACT

This paper provides a theoretical and numerical framework to investigate the interactions between domain walls and arrays of dislocations in ferroelectric single crystals. A phase-field approach is implemented in a non-linear finite element method to determine equilibrium solutions for the coupled electromechanical interactions between a domain wall and a dislocation array. The numerical simulations demonstrate the effect of the relative size and orientation of dislocations on 180° and 90° domain wall configurations. In addition, results for the pinning strength of dislocations in the case that domain walls move due the application of external electric field and shear stress are computed. The presented numerical results are compared with the findings reported for charged defects and it is shown that non-charged defects, such as dislocations, can also interact strongly with domain walls, and therefore affect the ferroelectric material behavior.

1. Introduction

Ferroelectrics constitute an important class of materials increasingly used in a wide variety of applications because of their coupled electromechanical behavior (Scott, 2007). To effectively and reliably harness the rich potential of ferroelectrics it is important to investigate their constitutive behavior at all scales. Ferroelectrics consist of domains of uniform polarization, and the boundaries between the domains, i.e. the domain walls, move under the influence of electric fields and stresses that are applied to the material. This domain wall motion is responsible for the significant non-linear dielectric, piezoelectric and elastic properties of ferroelectrics. In this context, defects such as oxygen vacancies, point charges, and dislocations play a crucial role in explaining important aspects of ferroelectric behavior since they interact with domain walls at submicron scales. For example, Yang et al. (1999) provide experimental observations on the pinning and bowing of domain walls near defects in ferroelectric crystals. In this context, oxygen vacancies have been reported to pin domain walls (Scott and Dawber, 2000). In addition, Brennan (1993, 1995) provides a theoretical description of the effect of charged defects in stabilizing domain configurations and in blocking their motion. Relevant numerical simulations have been performed by Su and Landis (2007), who further provide values for the critical applied electric field and shear stress required for the domain wall to break through an array of charged defects.

The role of dislocations in ferroelectric behavior, which is the focus of this paper, has been studied recently in the context of thin film applications. Specifically, Dai et al. (1996) examined the role of interface or misfit dislocations in a ferroelectric thin film/substrate structure during the formation of 90° domain boundaries. Their experiments showed that during cooling, the strains at the interface between the thin film and substrate are relaxed by the formation of domain boundaries. The strain reduction at the interface is accommodated by the interaction of misfit dislocations and the domain boundaries, which lowers the total energy of the system. Dai et al. also concluded that the dislocations act as pinning sites for the domain boundaries. In addition, Hu et al. (2003) focused on the role of interface dislocations in shaping the domain morphology of thin films. Their phenomenological model predicted the creation of domains around interfacial dislocations. Hu et al. further showed that the co-existence of dislocations and domain walls is energetically favored. Furthermore, Alpay et al. (2004) and Nagarajan et al. (2005) infer both experimentally and numerically that interface or misfit dislocations in ferroelectric thin films are responsible for the reduction of the exceptional dielectric properties of ferroelectrics due to the depolarizing fields caused by the interaction of the stress/strain fields of the dislocation with the ferroelectric constitutive behavior.

In a fashion similar to Su and Landis (2007), this paper investigates the interactions between domain walls and arrays of straight dislocations, which constitute a fundamental type of defect that commonly exists in materials. The results show that dislocations affect the equilibrium position of domain walls, change their shape, and act as pinning sites as domain walls move due to the

* Corresponding author. Tel.: +1 512 471 3924; fax: +1 512 471 5500.
E-mail address: landis@mail.utexas.edu (C.M. Landis).

0020-7683/$ - see front matter © 2008 Elsevier Ltd. All rights reserved.
doi:10.1016/j.ijsolstr.2008.11.021

application of external electrical and mechanical fields. The paper is organized as follows. Section 2 provides the theoretical background and constitutive equations, which are used in Section 3 to develop a non-linear finite element framework. Section 4 presents numerical results for 180° and 90° domain wall configurations near arrays of dislocations. These results demonstrate the effect of the dislocation size and orientation on the morphology of the domain walls, as well as on the critical electric field and stress values required for the walls to break through the dislocation sites. The computed results are compared to similar calculations reported by Su and Landis (2007) for charged defects. Finally, Section 5 offers a discussion of the results presented in this paper.

2. Theoretical model

Ferroelectric materials, below the Curie temperature, consist of one or more non-centrosymmetric phases, such as tetragonal or rhombohedral. Regions of uniform polarization called domains exist in these phases and they are separated by boundaries called domain walls. Domain walls are usually thin, with thickness on the order of a few lattice parameters (Scott, 2006). In barium titanate, which is the reference material in this paper, two kinds of domain walls are energetically favorable between two of the six tetragonal variants at room temperature; the 180° wall on a (100) plane and the 90° wall on a (110) plane. The polarization vectors are parallel and have opposite direction for 180° walls and they have a head-to-tail arrangement across the 90° wall. These two types of domain walls and their interactions with arrays of dislocations are modeled in this paper.

Given the importance of ferroelectric behavior in modern applications, particular interest has been given in developing models that can describe their basic characteristics at the microscopic level, e.g. phase transformations and domain nucleation and growth. Duan and Liu (2006) provide a review of the different modeling approaches that have been reported in the literature, such as microscopic displacive and order–disorder theories, first principles calculations, Monte Carlo methods, and molecular dynamics simulations, which are used to study various aspects of ferroelectric behavior. An interesting alternative to these methods is presented by a category of phenomenological models known as phase-field models (Chen, 2002). These models are generally based on the Landau–Ginsburg–Devonshire theory and have the potential of bridging atomistic computations and larger scale models. Phase-field models use a set of order parameters, which usually correspond to physically observable quantities such as the polarization vector in the case of ferroelectrics, to track changes in the materials microstructure. The order parameters are further assumed to be continuous across interfaces and therefore phase-field models are also referred to as diffuse interface models.

Phase-field models have been used extensively to describe various aspects of the ferroelectric behavior. For example, Cao and Cross (1991) used a phase-field model to analytically describe the twinning observed between the domain variants in ferroelectric phase transformations. Huang et al. (1997) also used phase-field theory to describe Ising and Bloch type 180° domain walls in barium titanate at different temperatures. In addition, phase-field models have been used for dynamic computations including the time-evolution of the polarization vector and the formation of domain structures. Ahluwalia and Cao (2000), Nambu and Sagala (1994), Hu and Chen (1997), Li et al. (2001), Schrade et al. (2007), Wang et al. (2004), Zhang and Bhattacharya (2005) and Zheng and Wang (2006) have all used various phase-field models to describe important aspects of the dynamics of domain formation and evolution in ferroelectric crystals.

The problem of interest in this paper, i.e. interactions of domain walls with dislocations, includes coupling between electrical and mechanical fields. The governing electrical, mechanical and phase-field equations used to solve this problem are presented next. Specifically, a general volume V and its surface S are considered for which mechanical equilibrium is stated as,

$$\sigma_{ji,j} + b_i = 0 \text{ in } V \tag{1}$$

$$\sigma_{ij} = \sigma_{ji} \text{ in } V \tag{2}$$

$$\sigma_{ji} n_j = t_i \text{ on } S \tag{3}$$

where σ_{ij} are the Cartesian components of the Cauchy stress tensor, b_i are the body forces per unit volume, n_i are the components of the unit vector normal to the surface, and t_i are the tractions applied to the surface. Summation over repeated indices is assumed and subscripts following commas represent partial differentiation with respect to the coordinate directions. Assuming linear kinematics, the following strain–displacement equations hold

$$\varepsilon_{ij} = \frac{1}{2}(u_{i,j} + u_{j,i}) \text{ in } V \tag{4}$$

where ε_{ij} are the strain tensor components and u_i the displacements. The electrostatic field equations are given as,

$$E_i = -\varphi_{,i} \text{ in } V \tag{5}$$

$$D_{i,i} - q = 0 \text{ in } V \tag{6}$$

$$D_i n_i = -\omega \text{ on } S \tag{7}$$

where E_i is the electric field, φ is the electric potential, q is the volume charge density, ω is the surface charge density, and D_i are the components of the electric displacement defined as

$$D_i = \kappa_o E_i + P_i \tag{8}$$

In Eq. (8), κ_o is the permittivity of free space and P_i are the components of the material polarization, which is the order parameter for the phase-field model used in this paper.

To solve the coupled electromechanical problem of interest, constitutive relationships must be obtained between stresses and strains, as well as between electric field and electric displacements. Su and Landis (2007) derive such constitutive laws by using a phase-field model and relevant thermodynamic considerations. In their model a material free energy form is assumed, which depends on mechanical strains and electric displacement components. It is further required that the free energy depends on the material polarization, i.e. the order parameter for phase-field modeling of ferroelectrics, and its gradients. Therefore, the free energy has the functional form given in Eq. (9)

$$\psi = \psi(\varepsilon_{ij}, D_i, P_i, P_{i,j}) \tag{9}$$

To account for the dependence of the free energy on the electric polarization and its gradients, Su and Landis postulate the existence of a set of micro-forces that do work on these additional independent variables. Therefore, they introduce a micro-force tensor ξ_{ij}, such that $\xi_{ji} n_j \dot{P}_i$ represents a power density across surfaces by neighboring microstructural configurations, an internal micro-force vector π_i, such that $\pi_i \dot{P}_i$ quantifies the power density expended by the material internally and therefore accounts for dissipation, and an external micro-force vector γ_i, such that $\gamma_i \dot{P}_i$ is a power density induced in the material by external sources. It is further assumed that these micro-forces are balanced in the material volume. Therefore this micro-force balance is stated as,

$$\xi_{ji,j} + \pi_i + \gamma_i = 0 \text{ in } V \tag{10}$$

This set of micro-forces also contributes to the total work on the system and consequently the following set of constitutive equations is obtained by using basic laws of thermodynamics and the procedure Coleman and Noll (1963)

$$\sigma_{ji} = \frac{\partial \psi}{\partial \varepsilon_{ij}}, \quad E_i = \frac{\partial \psi}{\partial D_i}, \quad \xi_{ji} = \frac{\partial \psi}{\partial P_{i,j}} \tag{11}$$

and

$$\eta_i = \frac{\partial \psi}{\partial P_i} \Rightarrow (\eta_i + \pi_i)\dot{P}_i \leqslant 0 \Rightarrow \pi_i = -\eta_i - \beta_{ij}\dot{P}_j \tag{12}$$

In Eq. (12), β_{ij} is the polarization viscosity tensor which must be positive definite. For the equilibrium simulations presented in this paper $\beta_{ij}\dot{P}_j = 0$. Eq. (11) provides the constitutive relationships needed to complete the set of equations that describes the coupled electromechanical behavior of ferroelectrics and to develop a finite element scheme.

Given the constitutive laws for the coupled electromechanical problem of interest, it is necessary to specify the material's free energy to find solutions. The chosen free energy form must be able to fit the characteristics of the ferroelectric behavior, namely the spontaneous polarization and strain and the general dielectric, piezoelectric and elastic properties. Eq. (13) presents the form of the free energy used in this paper

$$\begin{aligned}\psi = {} & \frac{1}{2}a_{ijkl}P_{i,j}P_{k,l} + \frac{1}{2}a_{ij}P_iP_j + \frac{1}{4}\bar{\bar{a}}_{ijkl}P_iP_jP_kP_l \\ & + \frac{1}{6}\bar{\bar{\bar{a}}}_{ijklmn}P_iP_jP_kP_lP_mP_n + \frac{1}{8}\bar{\bar{\bar{a}}}_{ijklmnrs}P_iP_jP_kP_lP_mP_nP_rP_s \\ & - b_{ijkl}\varepsilon_{ij}P_kP_l + \frac{1}{2}c_{ijkl}\varepsilon_{ij}\varepsilon_{kl} + \frac{1}{2}f_{ijklmn}\varepsilon_{ij}\varepsilon_{kl}P_mP_n \\ & + \frac{1}{2}g_{ijklmn}\varepsilon_{ij}P_kP_lP_mP_n + \frac{1}{2\kappa_o}(D_i - P_i)(D_i - P_i)\end{aligned} \tag{13}$$

This form comprises several terms that serve different goals. It agrees in structure with several other forms proposed in the literature but also has some key differences, which are pointed out here to show how they influence the computed results presented in this article. The first term in Eq. (12) represents the exchange or gradient energy, which penalizes large gradients of polarization and determines the thickness of the domain walls. This thickness is a characteristic length scale for the material of interest. The second line is a Landau-type expansion over the order parameter and creates the energy landscape associated with the polarization. The components of the third line are used to fit the anisotropic dielectric, elastic and piezoelectric properties near the spontaneous polarization and strain states. The sixth rank terms in this line were introduced by Su and Landis (2007) to fit the full set properties of the low symmetry phase in the spontaneous state. Finally, the last term appearing in the fourth line accounts for the stored energy of the free space occupied by the material.

3. Finite element implementation

Section 2 presents the fundamental balance laws and constitutive relationships that describe the coupled electromechanical behavior of ferroelectric materials. To obtain solutions to these equations, two-dimensional boundary value problems are formulated and solved using a non-linear finite element method. The nodal degrees of freedom in this formulation include the mechanical displacements, the material polarization components and the electric potential. From these degrees of freedom and the interpolations of the associated fields within the elements, the strains, polarization gradients and electric fields can be readily computed. A principal of virtual work can be formulated to specifically deal with the overall equilibrium of a given system configuration and loading,

$$\begin{aligned}\int_V (\sigma_{ji}\delta\varepsilon_{ij} + D_i\delta E_i + \eta_i\delta P_i + \xi_{ji}\delta P_{i,j})dV = {} & \int_V (b_i\delta u_i + q\delta\varphi + \gamma_i\delta P_i)dV \\ & + \int_S (t_i\delta u_i + \omega\delta\varphi + \xi_{ji}n_j\delta P_i)dS\end{aligned} \tag{14}$$

This principal of virtual work results in a set of non-linear algebraic equations for the nodal degrees of freedom. The solution to these equations is obtained using a standard Newton–Raphson scheme.

Fig. 1 shows a schematic of the boundary value problems formulated to obtain the results presented in this paper for 180° and 90° walls. The solid arrows in these models designate material polarization vectors. The dotted lines in Fig. 1 denote finite thickness domain walls and the dashed lines designate the cut-lines used to model the arrays of dislocations. Due to symmetry considerations the actual finite element model comprises one such dislocation with its core at the origin of the geometry. Periodic boundary conditions relating the degrees of freedom along the

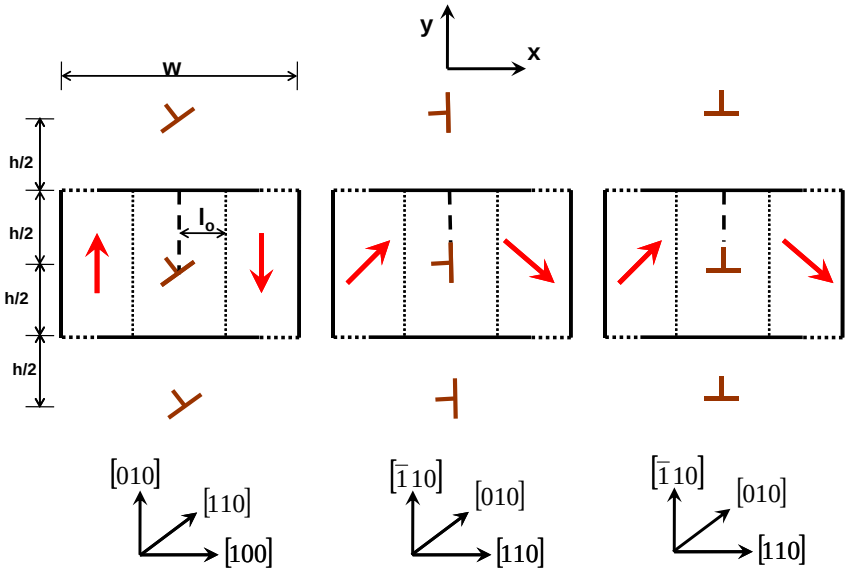

Fig. 1. The models used to investigate the interactions between domain walls and dislocations. The solid arrows denote the direction of the polarization vector, and therefore both 180° walls and 90° walls are modeled. The arrays of dislocations lie on the vertical axis. The distance between two dislocations in an array is equal to h. For a 180° wall on a (1 0 0) plane its interactions with arrays of dislocations in the [1 1 0] direction are considered. The 90° walls on a (1 1 0) plane interact with arrays of dislocations in the [$\bar{1}$ 1 0] and [1 1 0] direction. The finite element models have total height h and width w, while $2l_o$ is the domain wall width.

top and bottom surfaces of the modeled region are then imposed and are given in Eq. (15)

$$\begin{cases} u_x^t = u_x^b + \frac{\partial u_x}{\partial y} h \\ u_y^t = u_y^b + \frac{\partial u_y}{\partial y} h \\ \varphi^t = \varphi^b - Eh \\ P_x^t = P_x^b \\ P_y^t = P_y^b \end{cases} \tag{15}$$

where the superscripts t and b denote degrees of freedom along the top and bottom boundaries. The thickness of the domain walls is a characteristic material length scale and its value depends on the coefficients of the exchange energy terms in the form defined in Eq. (13), and on the energetic barriers between adjacent domain states. For the cases examined in this paper, the wall thickness is approximately equal to $2l_o$ where

$$l_o = \sqrt{\frac{a_o P_o}{E_o}} \tag{16}$$

In Eq. (16), a_o is a coefficient of the exchange energy term in the free energy form, P_o is the spontaneous polarization and E_o is the characteristic electrical field value required to cause homogenous switching when external electric field is applied in the opposite direction to a spontaneously polarized monodomain. Values for these parameters for barium titanate can be found in the Appendix. The width of the finite element models is then chosen to be equal to $100l_o$ to avoid any edge effects.

In Fig. 1 arrays of dislocations are drawn for both domain wall types. For a 180° wall on a (100) plane, arrays of dislocation in the [110] direction are considered. Their Burger's vectors are $\mathbf{b} = \frac{b}{\sqrt{2}}[1\,1\,0]$, where b is the dislocation size. For a 90° wall on a $(1\,1\,0)$ plane arrays of dislocations in the $[\bar{1}\,1\,0]$ and [110] directions are modeled and their corresponding Burger's vectors are $\mathbf{b} = \frac{b}{\sqrt{2}}[\bar{1}\,1\,0]$ and $\mathbf{b} = \frac{b}{\sqrt{2}}[1\,1\,0]$, respectively. The effect of the dislocation size on the configuration of both domain wall types is presented in Section 4.

Furthermore, it is noted that a significant difference exists between modeling of dislocations in the method presented in this article and similar ones reported in the literature. Specifically, Alpay et al. (2004) and Nagarajan et al. (2005) account for interface dislocations in their models by modifying the elastic part of the free energy functional and assuming dislocation fields from isotropic elasticity. Although these approaches provide some insight on the role of dislocations in the electromechanical interactions in ferroelectrics, they are based on linearity and isotropy assumptions that influence the results. In this paper, dislocations are constructed as displacement discontinuities across cuts in the crystal, in other words the dislocation solution is not imposed a priori but rather computed as part of the boundary value problem. The following boundary conditions are used to represent the dislocations

$$\begin{cases} u_x^+ = u_x^- + b_x \\ u_y^+ = u_y^- + b_y \\ \varphi^+ = \varphi^- \\ P_x^+ = P_x^- \\ P_y^+ = P_y^- \end{cases} \tag{17}$$

In Eq. (17) the + and − superscripts are used to designate quantities on the right and left of the dislocation cut, respectively. Within the finite element method the cut-line from the dislocation core to the upper boundary (the thick dashed line in Fig. 1) is modeled using two sets of nodes with identical positions. The dislocation is then created by enforcing the displacement boundary conditions that each node on the right side of the cut moves horizontally by b_x and vertically by b_y relative to its counterpart on the left side of the cut. These boundary conditions are imposed using the multi-point constraints listed in Eq. (17).

4. Domain wall interactions with dislocations

This section provides numerical results that show the effect of dislocations and external loading, such as electric field in the y-direction E_y and shear stress $\tau = \sigma_{xy}$, on the domain wall configurations. The applied electric field values are normalized with the characteristic field E_o, and the shear stress values with a characteristic stress $\sigma_o = E_o P_o / \varepsilon_o$, where ε_o is the spontaneous strain of a monodomain. In the case that no dislocations and no loads are present in the models shown in Fig. 1, both the 180° and the 90° domain walls are straight and their initial neutrally stable equilibrium position lies along the y-axis. The application of an external electric field for the 180° wall or electric field and shear stress for the 90° wall would force such walls to move indefinitely (except for special cancelling combinations of stress and electric field on the 90° wall).

Upon introducing an array of dislocations, Fig. 2 demonstrates the effects of their interaction on the 180° domain wall configuration. Specifically, P_y polarization distributions are plotted near a dislocation array with $\mathbf{b} = \frac{b}{\sqrt{2}}[1\,1\,0]$ and $b = 10\varepsilon_o l_o$. The distance h between the dislocations is equal to $100l_o$. Fig. 2 shows that within the phase-field framework, the domain wall is a diffuse zone where polarization changes smoothly between the adjacent domain states which are marked by solid white arrows. In addition, notice that the wall is kinked with respect to its original straight configuration. In fact, the numerical results reveal that as the dislocation size increases the kinking becomes more pronounced, as expected, indicating stronger interactions between the dislocations and the walls. Domain wall kinking, with a different morphology, has also been reported by Su and Landis (2007) for domain walls interacting with arrays of point charges. This demonstrates that the existence of non-charged defects, such as dislocations, cause similar electroelastic interactions in ferroelectrics. However, note that the apparent level of kinking of the domain wall observed in Fig. 2, and similar contour plots in this paper, is also affected by the different scales used in the x and y axes. It is further observed in Fig. 2 that the equilibrium position of the domain wall, which was initially placed along the y-axis, lies to the left of the arrays of dislocations when no electric field is applied. However, as the applied electrical field increases the domain wall shifts to the right until eventually it breaks through the array of dislocations. In Fig. 2, E_c is the critical value of the electrical field required to force the domain wall to break though, and for the dislocation size shown it is equal to $0.049E_o$. It is interesting to observe the shape of the kinking and note that the wall always bows towards the dislocation sites. This is a consequence of the details of the electrostatic fields near the defects. Hence, it is apparent that dislocations cause electromechanical interactions that change the shape of a 180° wall, and force the wall to be offset from the array when no external loads are applied. Note that all simulation results reported here correspond to equilibrium configurations. Therefore, the dynamics associated with the "breakthrough" phenomenon are not investigated and only the critical levels of electromechanical loading required to cause it are computed.

The effect of the dislocation size on the pinning strength of the array is shown in Fig. 3, which illustrates that larger Burger's vectors induce a greater critical electric field, i.e. the pinning strength of the dislocations increases. Note that the critical electric field values reported in Fig. 3 suggest a $1/h$ dependence. This observation agrees with calculations on the interactions between charge defects and domain walls, as reported by Su and Landis (2007).

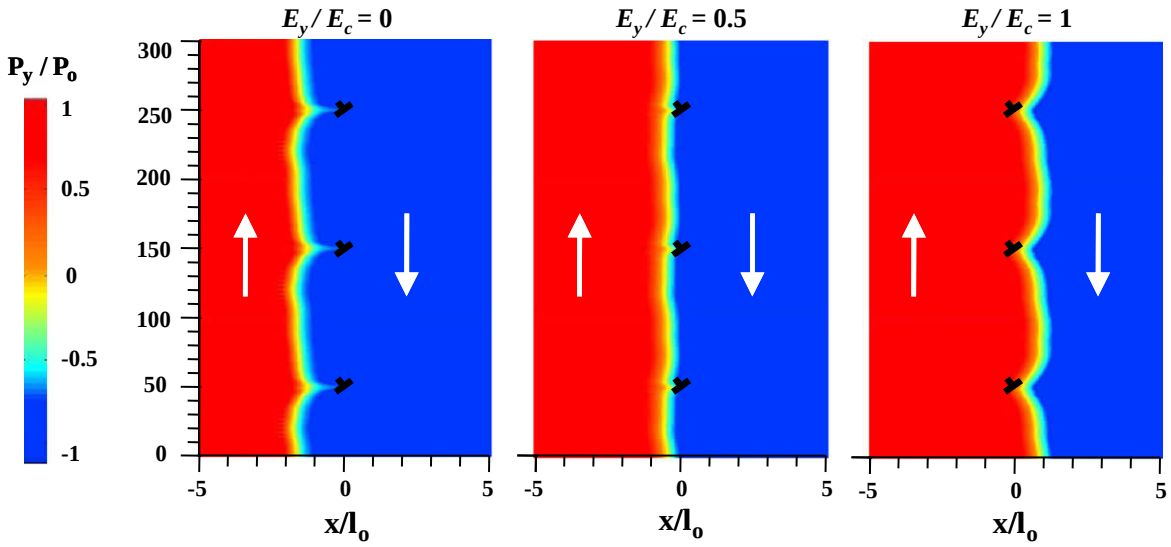

Fig. 2. Polarization distributions in the y-direction near a 180° domain wall interacting with an array of dislocations in the [1 1 0] direction. The x scale is normalized with l_o and the polarization values with P_o. The solid white arrows designate the direction of the polarization vector. Periodic boundary conditions are enforced on the lines at half the distance $h = 100l_o$ between the dislocations. For $E_y/E_c > 1$ the wall breaks through the dislocation.

Furthermore, the direction of the domain wall motion depends on the sign of the applied electric field. For the [1 1 0]-type dislocation orientation in the 180° domain wall case it is found that the equilibrium position of the wall lies to the left of the array, when no external loads are applied. Fig. 2 shows that if a positive electric field is applied, the wall moves towards the array and eventually passes through. However, the application of a negative electric field leads to a domain wall motion towards the opposite direction. In this case though, the results for $h = 100l_o$ displayed in the inset of Fig. 3 show that the computed pinning strength values are significantly smaller compared to the corresponding ones for positive applied electric field. Therefore, the results in Fig. 3 show that it is relatively easier for the domain wall to move away from the dislocation array due to a negative electric field than it is to pass through the array due to a positive electric field.

For a 90° domain wall, the interaction with an array of [1 1 0]-type dislocations are modeled, as shown in Fig. 1. When no external electric field or shear stress is applied the computed results

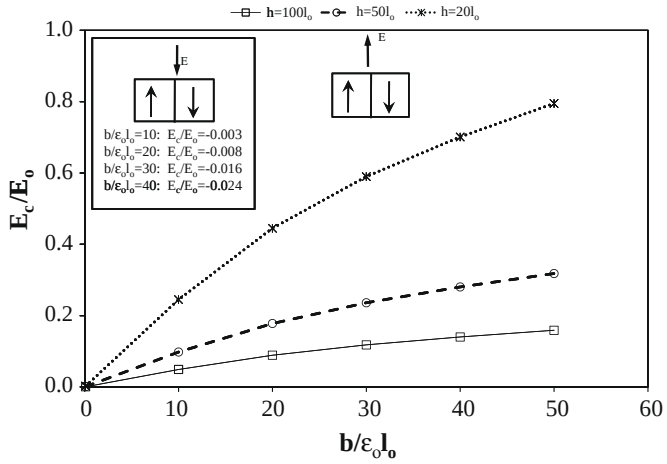

Fig. 3. The critical values of the positive electric field in the y-direction required to force a 180° domain wall to break through arrays of dislocations in the [1 1 0] direction for various values of the normalized Burger's vector and three values of the dislocation spacing h. The electric field values are normalized by E_o. Critical values are also given in the inset for negative applied electric field for $h = 100l_o$.

show that the domain wall equilibrium position lies to the left of the dislocation array with Burger's vectors $\mathbf{b} = \frac{b}{\sqrt{2}}[\bar{1}\,1\,0]$, as in the 180° wall case. Therefore, pinning strength values computed for domain wall motion away from the dislocation array are expected to be smaller than the corresponding values for motion towards the dislocations. However, for a 90° wall interacting with dislocations that have Burger's vectors $\mathbf{b} = \frac{b}{\sqrt{2}}[1\,1\,0]$ the domain wall equilibrium position, for no external loading, lies exactly on the dislocation array. Consequently, the pinning strength values computed for positive or negative applied field are expected to be the same from symmetry considerations.

Fig. 4 presents the critical electric field and shear stress values required to force a 90° domain wall to escape the local pinning action of the dislocation array for different values of the dislocation size. The $1/h$ pinning strength dependence is also found to apply for this case and therefore results for only $h = 100l_o$ are reported. Fig. 4 shows that as the dislocation size increases the pinning strength of dislocations measured either in terms of positive electric field or shear stress values also increases. As, expected, for dislocations with $\mathbf{b} = \frac{b}{\sqrt{2}}[\bar{1}\,1\,0]$ the corresponding pinning strength values computed for negative applied electric field are smaller than the values computed for positive field. In addition, it is observed that there is no difference between the pinning strength computed for positive or negative applied electric field for 90° walls interacting with an array of [1 1 0]-type dislocations. A comparison of the pinning strengths for all types of interactions between domain walls and dislocations is given later in this section.

Fig. 5 shows the effect of applied positive electric field on the configuration of a 90° wall interacting with an array of dislocations in the $[\bar{1}\,1\,0]$ direction. The electric field values in Fig. 5 are normalized with the critical value $E_c = 0.024E_o$, which causes the wall to break through the dislocation for a Burger's vector size $b = 10\varepsilon_o l_o$. As seen in this figure, for no applied electric field the electromechanical interactions between the domain wall and the dislocation cause significant kinking of the wall. Compared to the 180° wall the kinking of the wall is more pronounced for the same dislocation size. The equilibrium position of the 90° wall lies to the left of the array of dislocations and the application of positive electrical field causes the domain wall to shift to the right. When the applied field reaches the critical value E_c, the results shown in Fig. 5 illustrate the equilibrium position just before the wall breaks through

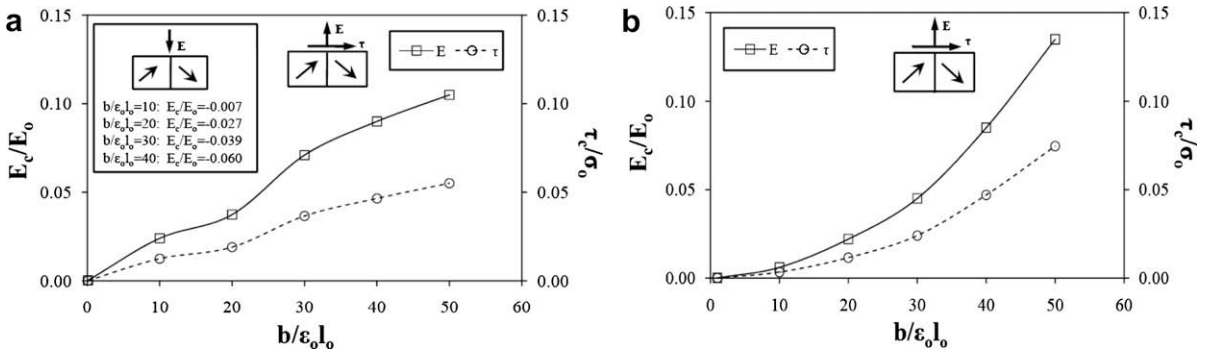

Fig. 4. The critical values of the electric field in the y-direction required to force a 90° domain wall to break through arrays of dislocations. (a) in the $[\bar{1}\,1\,0]$ direction (the inset gives the negative values computed for domain wall motion to the left) and (b) in the $[1\,1\,0]$ direction, for different values of the normalized dislocation size. The dislocation spacing in the arrays is $h = 100l_o$. The electric field values are normalized by E_o and the shear stress values with σ_o.

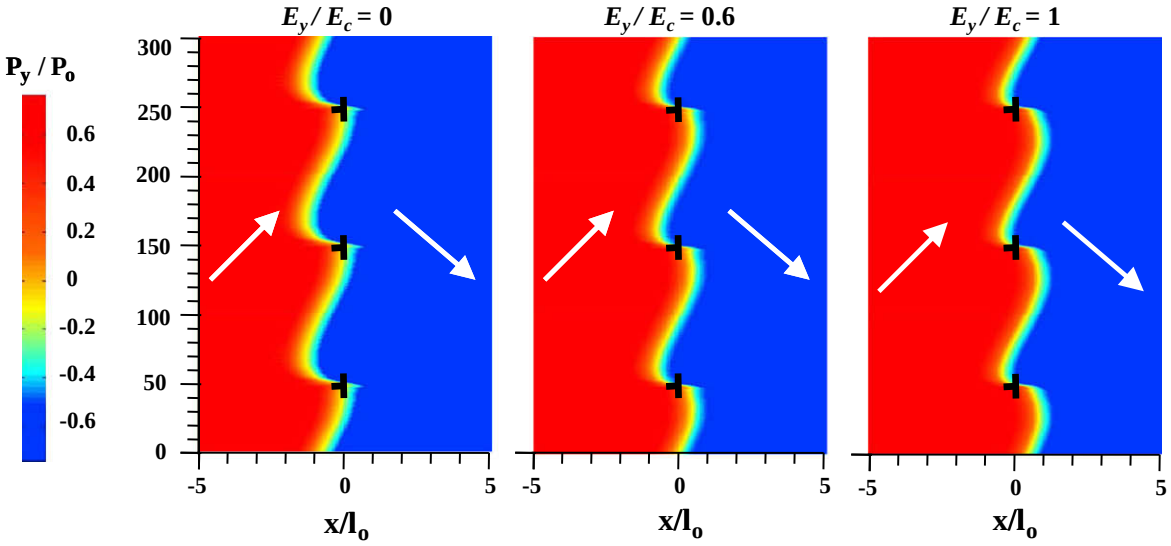

Fig. 5. Polarization distributions in the y-direction near a 90° domain wall interacting with an array of dislocations in the $[\bar{1}\,1\,0]$ direction having Burger's vectors size $b = 10\varepsilon_o l_o$. The x scale is normalized with l_o and the polarization values with P_o. The solid white arrows designate the direction of the polarization vector. Periodic boundary conditions are enforced on the lines at half the distance $h = 100l_o$ between the dislocations. For $E_y/E_c > 1$ the wall breaks through the dislocation.

the dislocation array. Similar results have been obtained for a 90° wall interacting with $[1\,1\,0]$-type dislocations and are presented in Fig. 6. Note that the equilibrium position of the domain wall in Fig. 6, for no applied electric field, lies exactly on top of the dislocation array. It is further noted that the effects on the domain wall caused by its interaction with the array of dislocations in the case that electric field is applied are very similar to the corresponding effects caused when only shear stresses are applied. This obervation agrees with the case of charged defects interacting with dislocations.

As mentioned before for 90° walls interacting with arrays of dislocations, the effects caused by the application of electric field E_y are similar to the corresponding effects caused by shear stresses σ_{xy}. In fact, Su and Landis (2007) noticed the same behavior and they proposed the existence of switching surfaces, which determine the critical values of combined electromechanical loading required for a 90° domain wall to break through the defect array. Fig. 7 presents such surfaces for various sizes of $[\bar{1}\,1\,0]$ and $[1\,1\,0]$-type dislocations interacting with a 90° wall. This figure agrees conceptually with the results computed by Su and Landis and indicates that as the dislocation size increases the critical values for the electric field, the shear stresses, or their combination also increases, and therefore the corresponding switching surface shifts outward. Fig. 7 indicates that for combined loading states that lie inside the area defined by the switching surfaces, the domain wall will return to its initial equilibrium position if the applied loading is removed, while for states that lie on the switching surfaces the domain wall breaks through the dislocation array.

The results presented for the interaction of domain walls with dislocations provide values for the pinning strength of dislocations for the case where the walls move due to the application of electromechanical loads. It was shown that the load direction, as well as the dislocation size and orientation affect the pinning strength of the dislocations. In addition, it is important to note that the spacing between adjacent dislocations also affects the critical electrical field values required to force domain walls to break through dislocations as shown in Fig. 3. Specifically, the presented numerical results for dislocation sizes in the range $0.1 < b/\varepsilon_o l_o < 50$ and spacings $10 < h/l_o < 100$ for both types of domain walls show that there is a $1/h$ dependence for the critical electrical field values. Similar observations had been made by Su and Landis (2007) for charged defect arrays. Dimensional analysis suggests that for a given material

$$\frac{E_c}{E_o} = f\left(\frac{b}{\varepsilon_o l_o}\right)\frac{b}{\varepsilon_o h} \tag{19}$$

where f is a dimensionless function of $b/\varepsilon_o l_o$. Fig. 8 plots the function f appearing in Eq. (19) for $h/l_o = 100$. This figure shows that the pin-

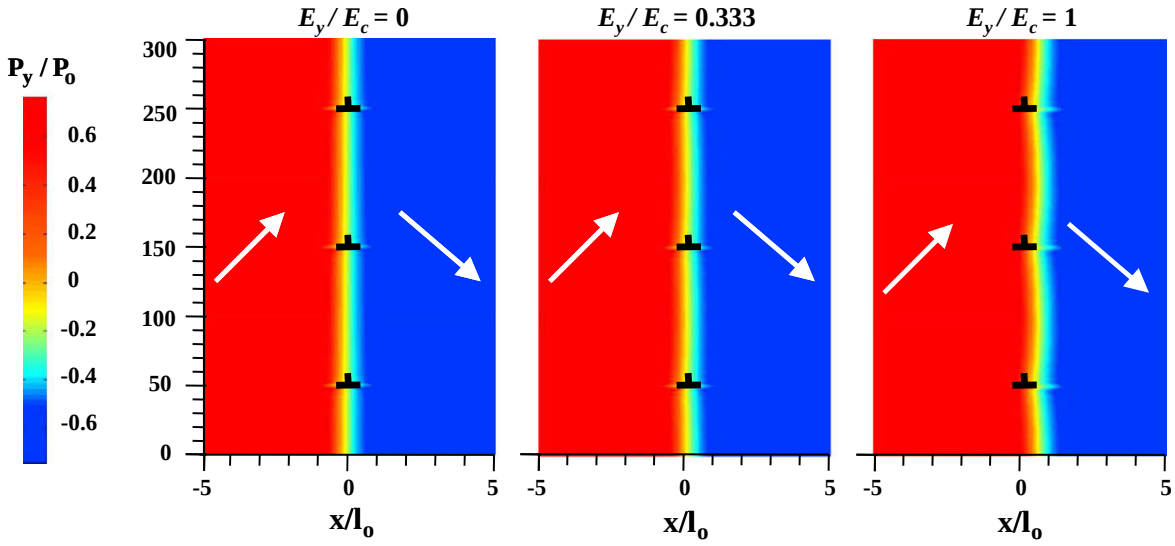

Fig. 6. Polarization distributions in the y-direction near a 90° domain wall interacting with an array of dislocations in the [1 1 0] direction having Burger's vectors size $b = 10\varepsilon_o l_o$. The x scale is normalized with l_o, the polarization values with P_o and the applied electric field values with the critical value $E_c = 0.06E_o$. The solid white arrows designate the direction of the polarization vector. Periodic boundary conditions are enforced on the lines at half the distance $h = 100l_o$ between the dislocations. For $E_y/E_c > 1$ the wall breaks through the dislocation.

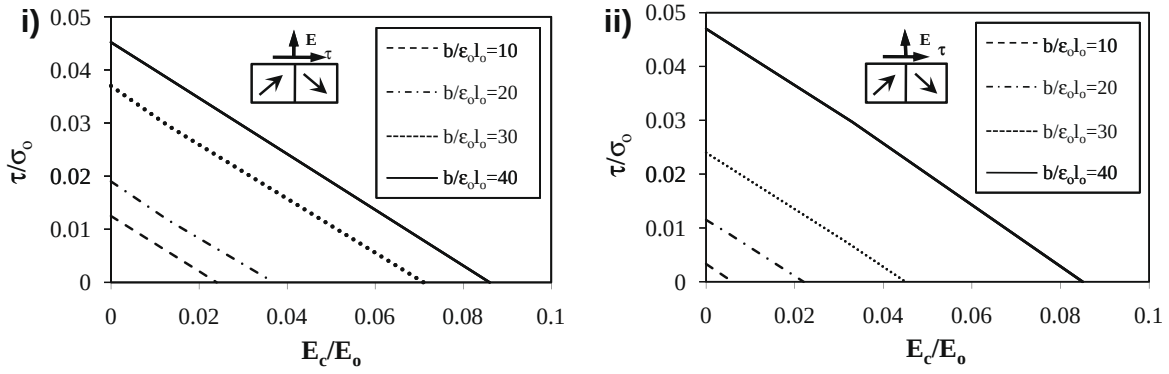

Fig. 7. Switching surfaces for 90° domain wall interacting with arrays of dislocations (i) in the [$\bar{1}$ 1 0] and (ii) in the [1 1 0] direction for various normalized sizes. The dislocation spacing is $h = 100l_o$. The computed linear relationship between the critical electric field and shear stress values required to break through the arrays agrees with the results reported by Su and Landis (2007).

ning strength values for dislocations interacting with 180° walls is larger compared to the corresponding values computed for 90° walls. Note that for [1 1 0]-type dislocations interacting with 90° walls, Fig. 8 suggests that $f \to 0$ as $b/\varepsilon_o l_o \to 0$.

5. Concluding remarks

This paper reports on computational modeling of the interactions between domain walls and arrays of dislocations in ferroelectric single crystals. The numerical framework is based on a phase-field model in conjunction with a non-linear finite element method. Numerical results are computed by solving coupled electromechanical boundary value problems simultaneously with the dislocation problem. The findings reported in this paper clearly show that dislocations affect the configuration of 180° and 90° domain walls. Specifically, it is observed that for both wall types the increase of the dislocation size causes more kinking and stronger electromechanical interactions. In addition, the results show that the interaction between domain walls and dislocations is affected by externally applied electric field and shear stresses. It is shown that the application of external fields, forces the walls to move, and that this motion is hindered by the dislocations. Values for the pinning strength of dislocations for both wall types are computed. Furthermore, the existence of switching surfaces is proposed for the determination of the pinning strength in terms of the applied electric field, shear stress and their combination for 90° walls, in agreement with similar results for charged defects. Overall, this paper provides quantitative predictions about the interactions of domain walls with dislocations, and provides a theoretical and numerical modeling framework that can be used to further elucidate the role of dislocations in ferroelectric behavior.

Acknowledgements

We gratefully acknowledge support for this work from NSF through Grant CMMI-0719071 and from ARO through Contract W911 NF-07-1-0495.

Appendix

Eq. (13) presented the general form of the Helmholtz free energy used in this paper. For a coordinate system aligned with the [1 0 0] direction, the specific form used to fit the dielectric, piezo-

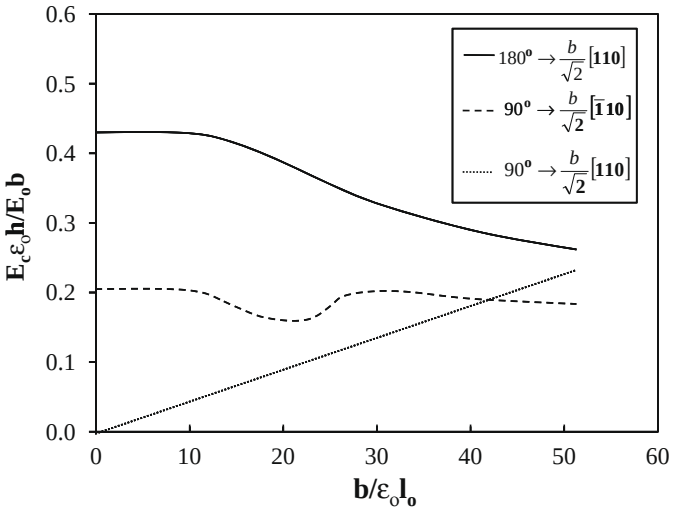

Fig. 8. The critical electric field required for 180° and 90° walls to break through arrays of dislocations as shown in Fig.1. The dimensionless quantity $f\left(\frac{b}{\varepsilon_o l_o}\right)$ given in Eq. (19) is plotted as a function of the normalized dislocation size $b/\varepsilon_o l_o$.

electric and elastic properties of ferroelectric single crystals that undergo a cubic to tetragonal phase transformation is taken from Su and Landis (2007) and is given next. Note that some typographical errors in the free energy and normalized constants that appeared in Su and Landis (2007) have been corrected here.

$$\begin{aligned}
\psi = {} & \frac{a_o}{2}(P_{1,1}^2+P_{2,2}^2+P_{3,3}^2+P_{1,2}^2+P_{2,1}^2+P_{1,3}^2+P_{3,1}^2+P_{2,3}^2+P_{3,2}^2)\\
& +\frac{a_1}{2}(P_1^2+P_2^2+P_3^2)+\frac{a_2}{4}(P_1^4+P_2^4+P_3^4)+\frac{a_3}{2}(P_1^2P_2^2+P_2^2P_3^2+P_1^2P_3^2)\\
& +\frac{a_4}{6}(P_1^6+P_2^6+P_3^6)+a_6(P_1^4(P_2^2+P_3^2)+P_2^4(P_1^2+P_3^2)+P_3^4(P_1^2+P_2^2)\\
& +\frac{a_5}{4}(P_1^4P_2^4+P_2^4P_3^4+P_1^4P_3^4)-\frac{b_1}{2}(\varepsilon_{11}P_1^2+\varepsilon_{22}P_2^2+\varepsilon_{33}P_3^2)\\
& -\frac{b_2}{2}((\varepsilon_{22}+\varepsilon_{33})P_1^2+(\varepsilon_{11}+\varepsilon_{33})P_2^2+(\varepsilon_{11}+\varepsilon_{22})P_3^2)\\
& -b_3((\varepsilon_{12}+\varepsilon_{21})P_1P_2+(\varepsilon_{13}+\varepsilon_{31})P_1P_3+(\varepsilon_{23}+\varepsilon_{32})P_2P_3)\\
& +\frac{c_1}{2}(\varepsilon_{11}^2+\varepsilon_{22}^2+\varepsilon_{33}^2)+c_2(\varepsilon_{11}\varepsilon_{22}+\varepsilon_{11}\varepsilon_{33}+\varepsilon_{22}\varepsilon_{33})\\
& +\frac{c_3}{2}(\varepsilon_{12}^2+\varepsilon_{21}^2+\varepsilon_{13}^2+\varepsilon_{31}^2+\varepsilon_{23}^2+\varepsilon_{32}^2)+\left(\frac{f_1}{2}\varepsilon_{11}^2+\frac{f_2}{2}(\varepsilon_{22}^2+\varepsilon_{33}^2)\right.\\
& +f_3(\varepsilon_{11}\varepsilon_{22}+\varepsilon_{11}\varepsilon_{33})+f_4\varepsilon_{22}\varepsilon_{33}+\frac{f_5}{2}(\varepsilon_{12}^2+\varepsilon_{21}^2+\varepsilon_{13}^2+\varepsilon_{31}^2)\\
& \left.+\frac{f_6}{2}(\varepsilon_{23}^2+\varepsilon_{32}^2)\right)P_1^2+\left(\frac{f_1}{2}\varepsilon_{22}^2+\frac{f_2}{2}(\varepsilon_{11}^2+\varepsilon_{33}^2)\right.\\
& +f_3(\varepsilon_{11}\varepsilon_{22}+\varepsilon_{22}\varepsilon_{33})+f_4\varepsilon_{11}\varepsilon_{33}+\frac{f_5}{2}(\varepsilon_{12}^2+\varepsilon_{21}^2+\varepsilon_{23}^2+\varepsilon_{32}^2)\\
& \left.+\frac{f_6}{2}(\varepsilon_{13}^2+\varepsilon_{31}^2)\right)P_2^2+\left(\frac{f_1}{2}\varepsilon_{33}^2+\frac{f_2}{2}(\varepsilon_{11}^2+\varepsilon_{22}^2)+f_3(\varepsilon_{11}\varepsilon_{33}+\varepsilon_{22}\varepsilon_{33})\right.\\
& +f_4\varepsilon_{11}\varepsilon_{22}+\frac{f_5}{2}(\varepsilon_{13}^2+\varepsilon_{31}^2+\varepsilon_{23}^2+\varepsilon_{32}^2)+\frac{f_6}{2}(\varepsilon_{12}^2+\varepsilon_{21}^2)\Big)P_3^2\\
& +\left(\frac{g_1}{4}\varepsilon_{11}+\frac{g_2}{4}(\varepsilon_{22}+\varepsilon_{33})\right)P_1^4+\left(\frac{g_1}{4}\varepsilon_{22}+\frac{g_2}{4}(\varepsilon_{11}+\varepsilon_{33})\right)P_2^4\\
& +\left(\frac{g_1}{4}\varepsilon_{33}+\frac{g_2}{4}(\varepsilon_{11}+\varepsilon_{22})\right)P_3^4+\frac{g_3}{4}(\varepsilon_{12}+\varepsilon_{21})(P_1P_2^3+P_2P_1^3)\\
& +\frac{g_3}{4}(\varepsilon_{13}+\varepsilon_{31})(P_1P_3^3+P_3P_1^3)+\frac{g_3}{4}(\varepsilon_{23}+\varepsilon_{32})(P_2P_3^3+P_3P_2^3)\\
& +\frac{1}{2\kappa_o}((D_1-P_1)^2+(D_2-P_2)^2)+(D_3-P_3)^2)
\end{aligned}$$

In the equation above $\kappa_o = 8.854\times10^{-12}$ F/m, and

$$a_1=-0.668325E_o/P_o,\quad a_2=-3.80563E_o/P_o^3,\quad a_3=0.78922E_o/P_o^3,$$

$$a_4=12.4421E_o/P_o^5,\quad a_5=368E_o/P_o^7,\quad a_6=0.134226E_o/P_o^5,$$

$$b_1=2.54138E_o/\varepsilon_oP_o,\quad b_2=1.74267E_o/\varepsilon_oP_o,\quad b_3=0.399353E_o/\varepsilon_oP_o,$$

$$c_1=2.04999\sigma_o/\varepsilon_o,\quad c_2=0.971673\sigma_o/\varepsilon_o,\quad c_3=1.27976\sigma_o/\varepsilon_o,$$

$$f_1=0.663581E_o/\varepsilon_o^2P_o,\quad f_2=0.841326e_o/\varepsilon_o^2P_o,\quad f_3=-0.170635E_o/\varepsilon_o^2P_o,$$

$$f_4=0.687281E_o/\varepsilon_o^2P_o,\quad f_5=0.10664E_o/\varepsilon_o^2P_o,\quad f_6=0.213294E_o/\varepsilon_o^2P_o,$$

$$g_1=-3.66149E_o/\varepsilon_oP_o^3,\quad g_2=6.27423E_o/\varepsilon_oP_o^3,\quad g_3=-1.21644E_o/\varepsilon_oP_o^3$$

where $\sigma_o = E_oP_o/\varepsilon_o = 692\times10^6$ N/m^2. In addition, $P_o = 0.26$ C/m^2, $\varepsilon_o = 0.0082$ and $E_o = 2.18247\times10^7$ V/m correspond to properties of monodomain single crystal barium titanate at room temperature.

The parameter a_o appearing in Eq. (17) determines the domain wall thickness. Hence, if $a_o = 1\times10^{-10}$ Vm^3/C then $l_o = 1$ nm, and therefore the wall has thickness equal to 2 nm which agrees with experimental observations (Scott, 2006). For this value of l_o, the maximum dislocation size investigated in this paper is on the order of 0.41 nm.

References

Ahluwalia, R., Cao, W., 2000. Influence of dipolar defects on switching behavior in ferroelectrics. Physical Review B 63, 1–4.

Alpay, S.P., Misirlioglu, I.B., Nagarajan, V., Ramesh, R., 2004. Can interface dislocations degrade ferroelectric properties? Applied Physics Letters 85, 2044–2046.

Brennan, C., 1993. Model of ferroelectric fatigue due to defect/domain interactions. Ferroelectrics 150, 199–208.

Brennan, C., 1995. Landau theory of thin ferroelectric films. Integrated Ferroelectrics 8, 335–346.

Cao, W., Cross, W., 1991. Theory of tetragonal twin structures in ferroelectric perovskites with a first-order phase transition. Physical Review B44, 5–12.

Chen, L.Q., 2002. Phase-field modeling for microstructure evolution. Annual Reviews in Materials Research 32, 113–140.

Coleman, R.D., Noll, W., 1963. The thermodynamics of elastic materials with heat conduction and viscosity. Archive for Rational Mechanics and Analysis 13, 167–178.

Dai, Z.R., Wang, Z.L., Duan, X.F., Zhang, J., 1996. Link-up of 90° domain boundaries with interface dislocations in $BaTiO_3/LaAlO_3$. Applied Physics Letters 68, 3093–3095.

Duan, W., Liu, Z.R., 2006. Theoretical modeling and simulations of perovskite ferroelectrics: from phenomenological approaches to ab initio. Current Opinion in Solid State & Materials Science 10, 40–51.

Hu, H.L., Chen, L.Q., 1997. Computer simulation of 90° ferroelectric domain formation in two-dimensions. Materials Science & Engineering A238, 182–191.

Hu, S.Y., Li, Y., Chen, L.Q., 2003. Effect of interfacial dislocations on ferroelectric phase stability and domain morphology in a thin film – a phase-field model. Journal of Applied Physics 94, 2542–2547.

Huang, X.R., Hu, X.B., Jiang, S.S., Feng, D., 1997. Theoretical model of 180° domain-wall structures and their transformation in ferroelectric perovskites. Physical Review B55, 5534–5537.

Li, Y.L., Hu, S.Y., Liu, Z.K., Chen, L.Q., 2001. Phase-field model of domain structures in ferroelectric thin films. Applied Physics Letters 78, 3878–3880.

Nagarajan, V., Jia, C.L., Kohlstedt, H., Waser, R., Misirlioglu, I.B., Alpay, S.P., Ramesh, R., 2005. Misfit dislocations in nanoscale ferroelectric heterostructures. Applied Physics Letters 86, 1–3.

Nambu, S., Sagala, D.A., 1994. Domain formation and elastic long-range interaction in ferroelectric perovskites. Physical Review B 50, 5838–5849.

Schrade, D., Müller, R., Xu, B.X., 2007. Domain evolution in ferroelectric materials: a continuum phase field model and finite element implementation. Computational Methods in Applied Mechanics and Engineering 196, 4365–4374.

Scott, J.F., 2006. Nanoferroelectrics: statics and dynamics. Journal of Physics: Condensed Matter, 18.

Scott, J.F., 2007. Applications of modern ferroelectrics. Science 315, 954–959.

Scott, J.F., Dawber, M., 2000. Oxygen-vacancy ordering as a fatigue mechanism in perovskite ferroelectrics. Applied Physics Letters 76, 3801–3803.

Su, Y., Landis, C.M., 2007. Continuum thermodynamics of ferroelectric domain evolution: theory, finite element implementation, and application to domain wall pinning. Journal of the Mechanics and Physics of Solids 55, 280–305.

Yang, T.J., Venkatraman, G., Swart, P.J., Mohideen, U., 1999. Direct observation of pinning and bowing of a single ferroelectric domain wall. Physical Review Letters 82 (20), 4106–4109.

Wang, J., Shi, S.Q., Chen, L.Q., Li, Y., Zhang, T.Y., 2004. Phase field simulations of ferroelectric/ferroelastic polarization switching. Acta Materialia 52, 749–764.

Zhang, W., Bhattacharya, K., 2005. A computational model of ferroelectric domains. Part I: Model formulation and domain switching. Acta Materialia 53, 185–198.

Zheng, Y., Wang, B., 2006. Simulation of interface dislocations effect on polarization distribution of ferroelectric thin films. Applied Physics Letters 88, 1–3.